CEMENT-IMPLANT INTERFACE FRACTURE FAILURE BY CRACK INITIATION DUE TO INTERFACE CAVITY STRESS CONCENTRATION

M. Haghpanahi & H. Ghomashchi

Abstract: *Nowadays total joint replacements are widely used in the world, so in average 800,000 joint surgeries are done yearly only in Europe and North America. However implant loosening is and remains as the major issue of all implant failures and therefore causes revision surgery procedures. Studies and experiments have identified poor fixation of implants most likely is the main cause of long term implant failure and in this case the cement-implant interface cavities are very effective due to resultant stress concentration . In this study the theory of this problem, continuum and mathematical equations for an inhomogeneous material by using Eshelby's equivalent inclusion method with a spherical void as a special type of inhomogenities is addressed and a new yield criterion with respect to the void's volume fraction is derived and changes in material elasticity tensor concerning Mori-Tanaka's theorem also determined, then by using finite element method and remeshing technique a macro scale cement-implant interface cavity is modeled and concerning the loss of strength due to void existence and the interface stress concentration, the crack initiation and propagation phenomenon is numerically investigated with respect to different orthopedic cement material properties. The results show that crack propagates at the interface at constant stress and strain by elastoplastic material and it propagates in cement bulk by considering elastic material properties for cement that both could cause implant loosening even in very small void's volume fractions in which there are no significant changes in cement yield stress and elasticity tensor according to analytical solution. But numerical simulation shows that when a homogenous cement structure is achieved via high vacuum mixing method, there is a uniform stress distribution in the cement structure and no stress concentration zone forms even at high stress levels and also there is no appropriate local site for crack initiation.*

Keywords*: mechanical loosening, implant, porous material, fracture, crack propagation, finite element*

1. Introduction

Nowadays Total Joint Replacements (TJR) are widely used in the world, so in average 800,000 joint surgeries are done yearly only in Europe and North America and implant loosening has the major contribution of all joint revision surgeries. Studies show that the poor fixation of implants is the main reason of long term implant failure and affect mechanical stability of joints. Regarding this subject,

orthopedic cement voids after transition of hardening phase have considerable influences [1].

The common way to mix the orthopedic cement is vacuum mixing which decreases the porosity of bone cement and cement-implant interface [2], [3], [4]. Several studies identified that the voids and cavities at the cement bulk cause the initiation and propagation of micro cracks lead to cement fracture. Fractography analyses show that cracks propagate more rapidly in fracture surfaces which contain larger voids [3]; therefore, reducing of porosity and eliminating the air bubbles are reasonable effort to improve the mechanical properties of acrylic bone cements [1], [2]. Voids and air bubbles make the cement-implant interface loosen at micro scale level, then the contact surface between bone and implant, in other words the

load bearing surface of bone and its ability to transfer the shear and tensile stresses will reduced and it is believed that separation of the stem-cement interface and fractures in the cement may initiate the initial loss of fixation of the implant [5], [6].

External loading, static or cyclic and/or monotonic or cumulative on surgical site when an inhomogeneity exists, causes stress concentration and initiates micro crack formation and growth; therefore, leads to fracture of material by fracture mechanics theories. Cracks will develop across the mating surfaces and after a while cause the mechanical loosening of implant.

2. Problem Formulation

Ductile failure mechanism which occurs in acrylic bone cements comprises void nucleation, void growth, and coalescence phenomenon, which the fracture plane is created by passing the last step and void coalescence. Void coalescence as the major consequences of last two stages highly depends on the state and magnitude of stress which defines the growth rate and also depends on strain hardening index and inter particle spacing [7], [8], [9].

Void formation causes internal separation in a homogeneous material. In engineering alloys voids are considered as the second phase of homogenous material called inhomogeneity just the same as void formation during the mixing process in orthopedic cements. According to this reason the void nucleation stage is eliminated and the strength of the material intrinsically reduces due to inter particle separation.

Generally inhomogeneities such as cavities, voids, inclusions, and dislocations affect the homogeneity of material and form specific stress and strain field around and inside the inhomogeneities, result in reduction of mechanical strength of materials. There is no unique and specific solution to confront with these problems and determine the stress, strain, and displacement fields around and inside the inhomogeneity i.e. an ellipsoidal void inside the homogeneous material can be considered as a very small crack and its influence in mechanical strength of the material can be modeled by the Griffith theory [10].

In this study by the general theory of inclusions and inhomogeneities and utilizing general expressions of elastic fields for given Eigen strain distributions, reduction of mechanical strength and the yield point due to presence of a spherical void are assessed. Then by using finite element method, stress concentration of a micro pore at cement-implant interface under external loading is modeled and crack formation and propagation for different material types for a micro pore are investigated.

Eigen strain is a generic name given to non elastic strains and eigen stress is a generic name given to self equilibrated internal stresses caused by one or several of eigen strains in bodies which are free from any other external forces and surface tractions. When an eigen strain is prescribed in a finite subdomain Ω in a homogeneous material D and it being zero in the matrix $D - \Omega$, then Ω called an inclusion and the elastic modulus of material are assumed to be homogenous. If the subdomain Ω in material D has elastic modulus different from those of matrix then Ω called an inhomogeneity. It is important to say a material containing inhomogeneity is free from any stress fields unless a load is applied and on the other hand a material containing inclusions is subjected to an internal stress field (eigen stress) even if it is free from any external tractions [10].

Eshelby pointed that the stress disturbance in an applied stress due to presence of an inhomogeneity can be simulated by an eigen strain caused by inclusion, when the eigen strain is chosen properly and this equivalency called Equivalent Inclusion Method.

A fictitious inclusion introduced as a subdomain Ω in domain D, then an eigen strain ε_{ij}^{*} is given in Ω and it is zero in $D - \Omega$. Since ε_{ij}^{*} is discontinuous on the boundary of domain Ω, some quantities may also be discontinuous on that boundary including the stress field which is continuous inside Ω and $D - \Omega$ but discontinuous at the interface between two domains, so the jump across the interface can be written as Eq. (1). (See [10])

$$[\sigma_{ij}] = \sigma_{ij}(out) - \sigma_{ij}(in) = C_{ijkl} \left\{ -C_{pqmn} \varepsilon_{mn}^{*} n_q n_l \frac{N_{kp}(\underline{n})}{D(\underline{n})} + \varepsilon_{kl}^{*} \right\} \tag{1}$$

Eq. (1) is useful for evaluating the stress just outside of the inclusion when the stress just inside the inclusion is known [1].

In this study an infinitely extended material with elastic modulus C_{ijkl} is considered containing a spherical domain Ω with elastic modulus C_{ijkl}^{*} called inhomogeneity and the disturbance in applied stress caused by presence of this inhomogeneity is investigated. If the applied stress at infinity denoted by σ_{ij}^{0}, then the corresponding strain is as Eq. (2).

$$\varepsilon_{ij}^{0} = \frac{1}{2}(u_{i,j}^{0} + u_{j,i}^{0}) \tag{2}$$

And the Hook's law can be written as Eq. (3) inside and outside the inhomogeneity.

$$\sigma_{ij}^{0} + \sigma_{ij} = C_{ijkl}^{*}(u_{k,l}^{0} + u_{k,l}) \qquad in \ \Omega$$
$$\sigma_{ij}^{0} + \sigma_{ij} = C_{ijkl}(u_{k,l}^{0} + u_{k,l}) \qquad in \ D - \Omega \tag{3}$$

Using Eshelby's equivalent inclusion method, the stress disturbance in an inhomogeneous material can be simulated by an arbitrary eigen strain caused by an

inclusion occupied the domain Ω of body D, concerning the fact that there is no internal Eigen strain for the inhomogeneity, so first term of Eq. (3) can be written as Eq. (4).

$$\sigma_{ij}^0 + \sigma_{ij} = C_{ijkl}(u_{k,l}^0 + u_{k,l} - \varepsilon_{kl}^*) \qquad in \ \Omega \qquad (4)$$

Then the necessary and sufficient condition for equivalency of stresses and strains inside Ω is as Eq. (5) or Eq. (6).

$$\sigma_{ij}^0 + \sigma_{ij} = C_{ijkl}^*(\varepsilon_{kl}^0 + S_{klmn}\varepsilon_{mn}^*) = C_{ijkl}(\varepsilon_{kl}^0 + S_{klmn}\varepsilon_{mn}^* - \varepsilon_{kl}^*)$$

Since both matrix and inhomogeneity are considered isotropic then C_{ijkl} can be expressed in terms of Lame constants.

$$\sigma_{ij}^0 + \sigma_{ij} = 2\mu(\varepsilon_{ij}^0 + S_{ijmn}\varepsilon_{mn}^* - \varepsilon_{ij}^*) + \lambda\delta_{ij}(\varepsilon_{kk}^0 + S_{kkmn}\varepsilon_{mn}^* - \varepsilon_{kk}^*) \qquad (10)$$

Eq. (10) is used to determine the stress field inside the inclusion; hence all the included terms in Eq. (10)

$$2\mu^*(\varepsilon_{ij}^0 + \varepsilon_{ij}) + \lambda^*\delta_{ij}(\varepsilon_{kk}^0 + \varepsilon_{kk}) = 2\mu(\varepsilon_{ij}^0 + \varepsilon_{ij} - \varepsilon_{ij}^*) + \lambda\delta_{ij}(\varepsilon_{kk}^0 + \varepsilon_{kk} - \varepsilon_{kk}^*) \qquad (11)$$

And by introducing deviatoric strains as mentioned in set of Eq. (12); Eq. (13) and Eq. (14) derived from Eq. (11).

$$\varepsilon_{ij}'^0 = \varepsilon_{ij}^0 - \frac{\delta_{ij}\varepsilon_{kk}^0}{3}$$

$$\varepsilon_{ij}'^* = \varepsilon_{ij}^* - \frac{\delta_{ij}\varepsilon_{kk}^*}{3} \qquad (12)$$

$$\varepsilon_{ij}' = \varepsilon_{ij} - \frac{\delta_{ij}\varepsilon_{kk}}{3}$$

$$2\mu^*(\varepsilon_{ij}'^0 + \varepsilon_{ij}') = 2\mu(\varepsilon_{ij}'^0 + \varepsilon_{ij}' - \varepsilon_{ij}'^*) \qquad (13)$$

$$k^*(\varepsilon_{kk}^0 + \varepsilon_{kk}) = k(\varepsilon_{kk}^0 + \varepsilon_{kk} - \varepsilon_{kk}^*) \qquad (14)$$

Expressions for the Eshelby tensor of ellipsoidal inclusions are independent of material symmetry and properties of inclusions [11]. Expressions for the Eshelby tensor of spheroidal inclusions in an isotropic matrix are given in [10] (see Appendix A for Eshelby tensor of an ellipsoidal inclusion in isotropic matrix), therefore using permutation in Eq. (7) yields the following results.

$$\varepsilon_{kk} = \varepsilon_{kk}^* \frac{(1+\nu)}{3(1-\nu)} \qquad (15)$$

Then,

$$\varepsilon_{ij}' = \varepsilon_{ij}'^* \frac{(8-10\nu)}{15(1-\nu)} \qquad (16)$$

$$C_{ijkl}^*(u_{k,l}^0 + u_{k,l}) = C_{ijkl}(u_{k,l}^0 + u_{k,l} - \varepsilon_{kl}^*) \qquad (5)$$

$$C_{ijkl}^*(\varepsilon_{kl}^0 + \varepsilon_{kl}) = C_{ijkl}(\varepsilon_{kl}^0 + \varepsilon_{kl} - \varepsilon_{kl}^*) \qquad (6)$$

By introducing Eshelby tensor S_{ijkl}, Eq. (8) yields from Eq. (6).

$$\varepsilon_{kl} = \frac{1}{2}(u_{k,l} + u_{l,k}) = S_{klmn}\varepsilon_{mn}^* \qquad (7)$$

$$\sigma_{ij}^0 + \sigma_{ij} = C_{ijkl}^*(\varepsilon_{kl}^0 + S_{klmn}\varepsilon_{mn}^*) = C_{ijkl}(\varepsilon_{kl}^0 + S_{klmn}\varepsilon_{mn}^* - \varepsilon_{kl}^*) \qquad in \ \Omega \qquad (8)$$

$$C_{ijkl} = \lambda\delta_{ij}\delta_{kl} + \mu(\delta_{ik}\delta_{jl} + \delta_{il}\delta_{jk}) \qquad (9)$$

That reforms Eq. (8) to Eq. (10).

should be determined as well. Eq. (6) can be written as follow.

With the aid of this last result, it follows from Eq. (13) that:

$$\varepsilon_{ij}'^* = \frac{15\varepsilon_{ij}'^0(\mu^* - \mu)(1-\nu)}{[(5\nu-7)\mu - (8-10\nu)\mu^*]} \qquad (17)$$

Substituting Eq. (15) in Eq. (14) yields:

$$\varepsilon_{kk}^* = \frac{3\varepsilon_{kk}^0(k^* - k)(1-\nu)}{[(4\nu-2)k - (1+\nu)k^*]} \qquad (18)$$

In view of the fact that in this study a void is under consideration, so it is not needed to express material properties are denoted by a superscript asterisk [*]. Eigen strain is determined by combination of two Eq. (17) and Eq. (18).

$$\varepsilon_{ij}^* = \frac{15\mu(\nu-1)\varepsilon_{ij}'^0}{(5\nu-7)\mu} + \frac{\delta_{ij}k(\nu-1)\varepsilon_{kk}^0}{(4\nu-2)k} \qquad (19)$$

Substituting Eigen strains tensor derived from Eq. (19) in Eq. (10), the fictitious stress field tensor inside the void is determined and substitution the result in Eq. (1) yields the stress field just outside of the void.

In this analytical case study, a macro spherical void with radius of 500μ in a cube shape orthopedic cement bulk with equal dimensions of 5 mm under applied tension σ in the x_3 direction is investigated. With the aid of Eq. (19) to calculate the Eigen strain field and

using Eq. (1), the stress tensor just outside of the void is determined. Principal axes and principal stresses are derived as shown in Eq. (20) & (21) and by assuming octahedral shear stress criterion (See Eq. (22)), a yield

$$\left\{ \frac{-2\mu}{3k} + \frac{\mu(5\nu-2)}{3k(2\nu-1)} + \frac{15(1-\nu)}{(5\nu-7)} - \frac{3\lambda\mu(1-\nu)}{2k(\lambda+2\mu)(2\nu-1)} \right\} = Q \tag{21}$$

Using octahedral shear stress criterion, results;

$$\tau_{oct} = \frac{1}{3}\left[(\sigma_1-\sigma_2)^2 + (\sigma_2-\sigma_3)^2 + (\sigma_3-\sigma_1)^2 \right]^{1/2} \tag{22}$$

$$\tau_{oct} = \frac{\sqrt{2}}{3}|\sigma.Q|$$

And:

$$\tau_{oct} = 0.47\,\sigma_{yp} \tag{23}$$

These equations were derived under assumption that the inhomogeneities are dilutely dispersed in the matrix and do not feel any affects due to their neighbors, it means that they are loaded by the unperturbed applied stress or applied strain and accordingly. Moreover it is assumed that the inhomogeneities are dispersed in the matrix with volume fraction equal to the volume fraction of the matrix and it means a completely semi porous material, so these equations are independent of inhomogeneity volume fraction. But in reality they are not independent of the inclusion (inhomogeneity) volume fraction (ξ), so for including ξ in our calculation and determine a new yield criterion, an exponential curve fitting procedure is down in curve fitting toolbox of MATLAB 7.1 software package and correlation between ξ and Q is derived as shown in Eq. (24).

$$Q = a.e^{b.\xi} \tag{24}$$

Where: a =1 & b= 0.8176, which fits the best for $0 \le \xi \le 0.5$.

Then the new yield criterion will be defined as:

$$E_M^* = E^{(m)}\left\{ I - \xi[(E^{(i)}-E^{(m)})(S-\xi(S-I)) + E^{(m)}]^{-1}[E^{(i)}-E^{(m)}] \right\}^{-1} \tag{26}$$

Where can be easily modified for porous materials by letting $\mathbf{E}^{(i)} \to 0$ to give:

$$E_{M,por}^* = E^{(m)}\left[I + \frac{\xi}{1-\xi}(I-S)^{-1} \right]^{-1} \tag{27}$$

And this elasticity tensor should be applied as the material elasticity when the stress disturbance due to a void existence in relatively porous material with $\xi \le 0.25$ is under consideration. In this investigation, with regards to our problem a hemispherical interface void is considered and with respect to the dimensions of the physical model which previously mentioned, the void's volume fraction is determined as 1.048 E-3 by the following formula.

point drop function with respect to void volume fraction (ξ) is determined as shown in Eq.(25).

$$\sigma_1(out) - \sigma_3(out) = \sigma_2(out) - \sigma_3(out) = \sigma.Q \tag{20}$$

Where $\sigma_1, \sigma_2, \sigma_3$ are principal stresses and Q is:

$$\sigma_{yp}^* = \frac{\sigma_{yp}}{e^{(0.8176)\xi}} \tag{25}$$

In reality, micro and macro pores are formed while mixing the orthopedic cement and remain within the hardened cement (see Fig. 1) and there are interactions between the voids when external loading is applied, so evaluating the stress disturbance and the strength reduction due void existence in a relatively porous medium by above mentioned equations are necessary but not sufficient, so changes in material elasticity also should be considered.
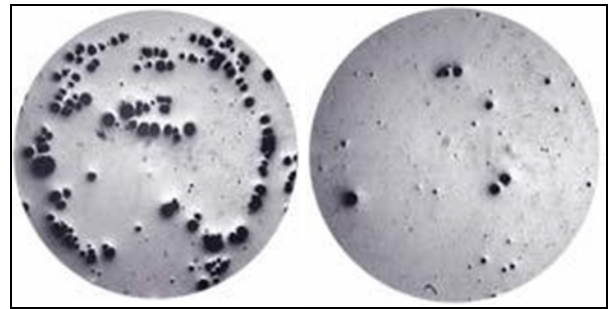

Fig. 1. Macro and micro voids within the hardened cement

There are different approaches and approximation for behavior of materials with inclusion volume fractions more than a few percent and one suitable approximation is Mori-Tanaka-Type estimation theorem in which the overall Mori-Tanaka's elasticity tensor is describe as [11]:

$$\xi = \frac{\Omega^i}{\Omega^i + \Omega^m} \tag{28}$$

Then by applying the new yield point criterion from Eq. (25), the new yield stress for the cement in this case is determined as $\sigma_{yp}^* = 109.9$ MPa. It can be readily seen from the result that there is no significant and sensible difference between homogenous material yield stress and inhomogeneous one concerning current void size and calculated volume fraction. Obviously when the porosity and thus the void's volume fraction increase, the yield stress of the material decreases as shown in Eq. (25). Moreover changes in material elasticity also with respect to current void size and

volume fraction should be investigated and as mentioned before the authors choose the Mori-Tanaka's theorem. According to Mori-Tanaka's theorem, changes in elasticity tensor of a porous

$$
\mathbf{E}^{*}_{\mathrm{M,por}} = 200E + 06 \begin{bmatrix} 0.9978 & -0.0002 & -0.0002 & 0 & 0 & 0 \\ -0.0002 & 0.9978 & -0.0002 & 0 & 0 & 0 \\ -0.0002 & -0.0002 & 0.9978 & 0 & 0 & 0 \\ 0 & 0 & 0 & 0.9986 & 0 & 0 \\ 0 & 0 & 0 & 0 & 0.9986 & 0 \\ 0 & 0 & 0 & 0 & 0 & 0.9986 \end{bmatrix} \tag{29}
$$

Above matrix shows that there are also no significant differences in elastic properties in both normal and shear direction between a homogenous and inhomogeneous material with current void size and the elastic properties are also in accordance with each other more than 99%. This analytical investigation shows that there are no significant differences between homogeneous cement and inhomogeneous one when only a single spherical macro void with radius of 500μ exists, but clinical and experimental observations and also fractography analyses show that the crack propagation and fracture occurred in cements which contain voids, pores and air bubbles and these two results are not in accordance with each other. So a numerical simulation is done to check whether the inhomogeneity/void existence affects the total strength of the material.

3. Numerical Method with Remeshing

In this study a linear incremental finite element method and an incremental crack simulation process by a hybrid software package FRANC2D is used for numerical solution which combines modeling, mesh generation, primary finite element analysis, and more important fracture mechanics. Via this software package the stress concentration at the cement-implant interface and moreover crack nucleation and propagation under external loading is investigated for both purely elastic and elastoplastic materials. The geometry used in the model is the cross sectional area of the idealized cylindrical cemented hip stem surrounded by cortical bone. For simplicity, a two dimensional micro scale FE model comprising cortical bone, cement, implant, and hemispherical interface void is considered as indicated with dashed line in Fig. 2 and the gross model dimensions are chosen according to [12] and [13]. As shown in Fig. 2 the cement is bonded by peripheral protection of bone that does not allow excessive large deformation and this assumption should be considered in every two dimensional modeling of this region and ignoring this matter, leads to underestimation the results because of inadequate stiffness of revised joint. In this study, assuming this peripheral bonding is necessary because it can confine the unstable cavity growth and excessive strains in low stress levels. In order to model this peripheral bonding, another rectangular region with cortical bone properties is submodeled and glued to the original FE model

material are determined by Eq. (27) and applying it to our inhomogeneous material leads to following result.

Fig.3 (a). In FE model initial void radius R_0 is 500μ and the ratio of initial void radius to cement cell width is $(R_0/L) = 0.1$ and regardless of peripheral bonding layer's width, the ratio of width to height of cement cell is $(L/H) = 1$.
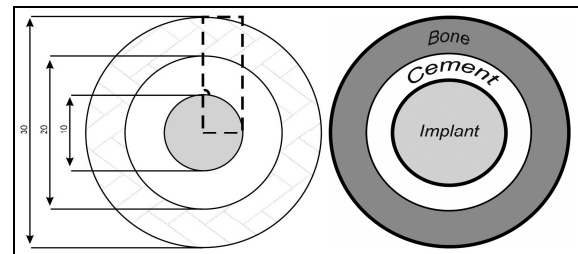

Fig. 2. Gross model dimensions and FE model region indicated by dashed line

Tab. 1. Material properties of FE model

Material	Elastic Modulus (MPa)	Yield Stress (MPa)	Poisson's Ratio
Implant (Cobalt chrome)	≈ 200000	-	0.3
Cortical Bone	≈ 20000	-	0.3
Cement (PMMA)	≈ 2000	110	0.3

Cortical bone and implant (Cobalt-Chrome alloy) are considered homogeneous, isotropic and linearly elastic and orthopedic cement (PMMA) is also considered homogeneous and isotropic, but at first it is considered as a linear elastic material and secondly, nonlinear elastoplastic behavior with $(\sigma_y/E) = 0.055$ is applied.

The inhomogeneity (macro void) is modeled separately in the model. Material properties assigned to the model are mentioned in Table 1, cited in [14] and [15]. Model is mapped meshed with quadrilateral eight node isoparametric elements. By use of plane of symmetry the results can be extended to the left half of the model, hence symmetric boundary condition is applied to the left edge of the model, and right edge of the main model is protected by the peripheral bonding layer to limit the excessive large deformation and nodes at the lower edge are limited to zero displacement in both x and y directions. External loading is applied in form of axial tensile stresses five times more than cement's yield stress $((\sigma_2/\sigma_y) = 5)$ in y direction on the upper edge of the model.
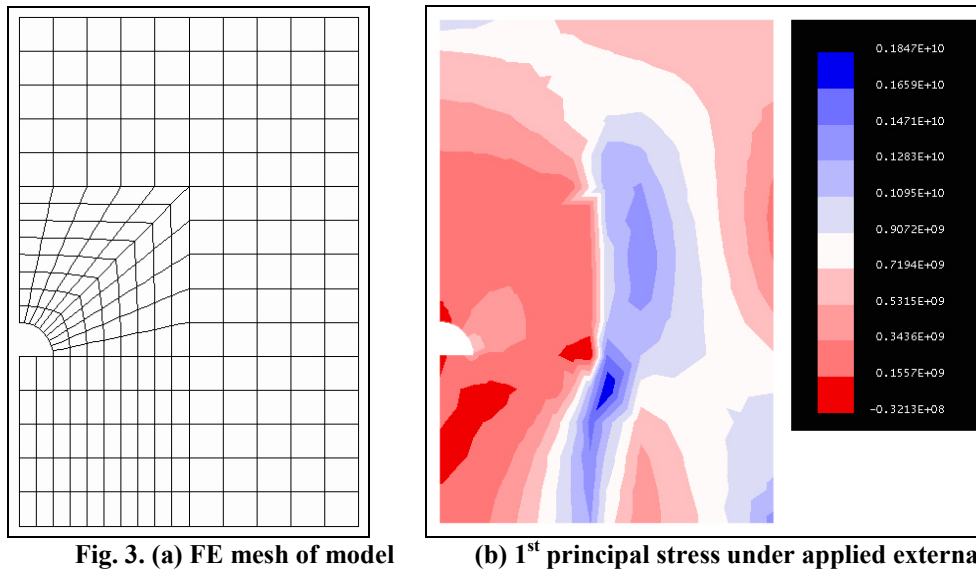
Fig. 3. (a) FE mesh of model   **(b) 1st principal stress under applied external loading**

First principal stress is shown in Fig.3 (b) as a result of this type of external loading; stress concentration in the cement structure at the mating surface can be readily seen. The stress concentration can be interpreted from two different aspects; first, as discussed in previous part inhomogeneities including voids, air bubbles and cavities may reduce, although in a small amount, the total strength of material that cause crack nucleation and initiation, on the other hand, high stress levels due to cavity existence at site itself could cause crack formation. An incremental linear elastic fracture mechanics is used for numerical solution. Local damage and crack growth are modeled by an integrated remeshing technique to overcome convergence problem caused by mesh distortion. The crack simulation process is an incremental process where a series of steps is repeated for a progression of the cracked model. Each iteration in the process relies on previously computed results, and represents one crack configuration.

4. Results

Two types of analyses have been done on this model depend on acrylic cement's material properties during external loading and propagation paths were compared with each other. As discussed before the stress concentration site is a reasonable region for crack nucleation which acts as test sample machining notch. So the first crack propagation path is defined at the cement-implant interface Fig.4. Moreover experiments show that the fracture originated from already existing cracks or surface (internal and external) discontinuities. Based on orthopedic cement material properties two analyses have been done, first considering purely elastic material and then an elastoplastic one. Cement's material properties are also listed in Table.1, for first analysis only the Young's modulus and Poisson's ratio are used but for materially nonlinear analysis the elastic properties plus yield stress are used and kinematic hardening is also considered.
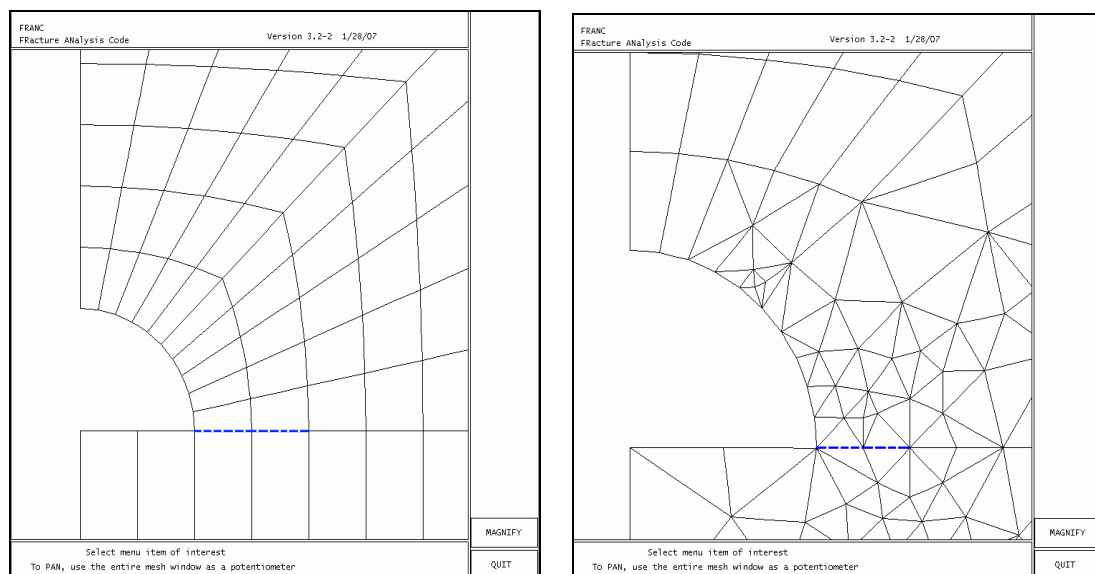

Fig. 4. 1st crack propagation path along the interface
(Singular elements after mesh modification are shown at crack tip)

For purely elastic material, the primary crack path is defined as shown in Fig.4, mesh modification is done to refine mesh along the path and create singular elements at crack tip. The deformed mesh (Fig. 5(a))

and stress field (1ˢᵗ principal stress) in the model (Fig. 5(b)) are obtained after loading and high stress levels at the crack tip can be seen that we will discuss about it later.
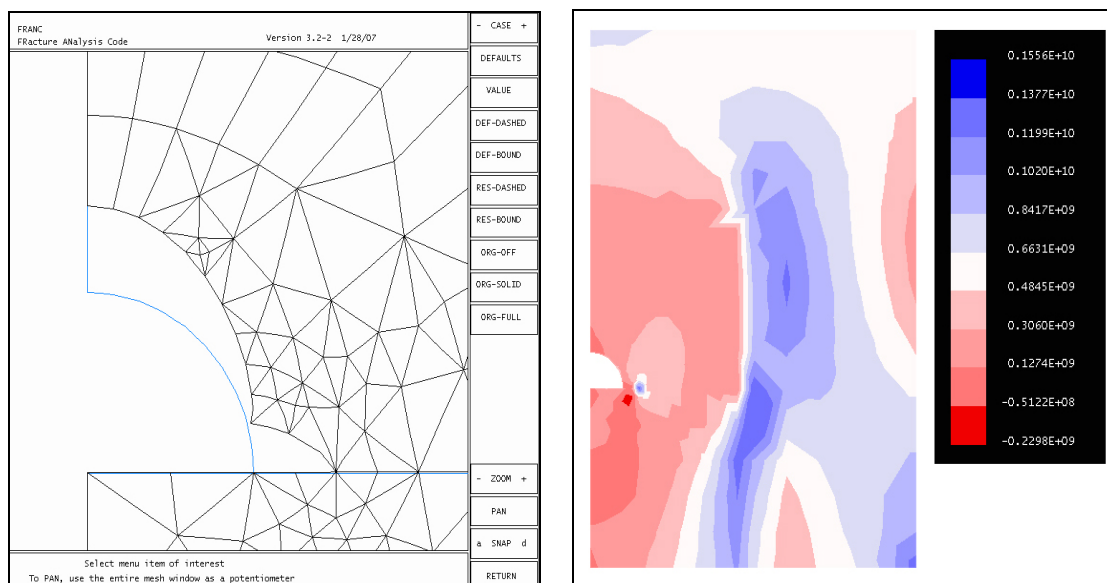

Fig. 5. (a) Deformed mesh at 1ˢᵗ step of crack propagation   (b) 1ˢᵗ principal stress at 1ˢᵗ step of crack propagation

There are different theories to predict in which direction the crack moves on, such as Sigma-Theta Maximum theory which states that it will move in the direction of maximum circumferential stress around the crack tip when a critical value of stress is reached or G-Theta Maximum theory that sates the crack will move in the direction of maximum energy release rate when a critical value of energy release rate is reached or The Minimum Strain Energy Density (S Minimum) theory which states that the crack will move in the direction where strain energy density is minimum when a critical value is reached. So this program automatically predicts in which direction the cracks move on and

propagate. For the second step for purely elastic material this program predicts that the crack will moves on the path shown in Fig.6 (a). Automatically remeshing technique is applied to the model in which the values of field quantities in the old mesh were transferred to new mesh and then mesh modification is done to refine mesh and create singular elements at crack tip location Fig.6 (b). Again another analysis has been done and the deformed mesh and 1ˢᵗ principal stress contours obtained (Fig. 7). This procedure again continued up to 4 steps and the results are shown in Fig. 8) to Fig. 11 and final crack propagation path is as shown in Fig. 12.
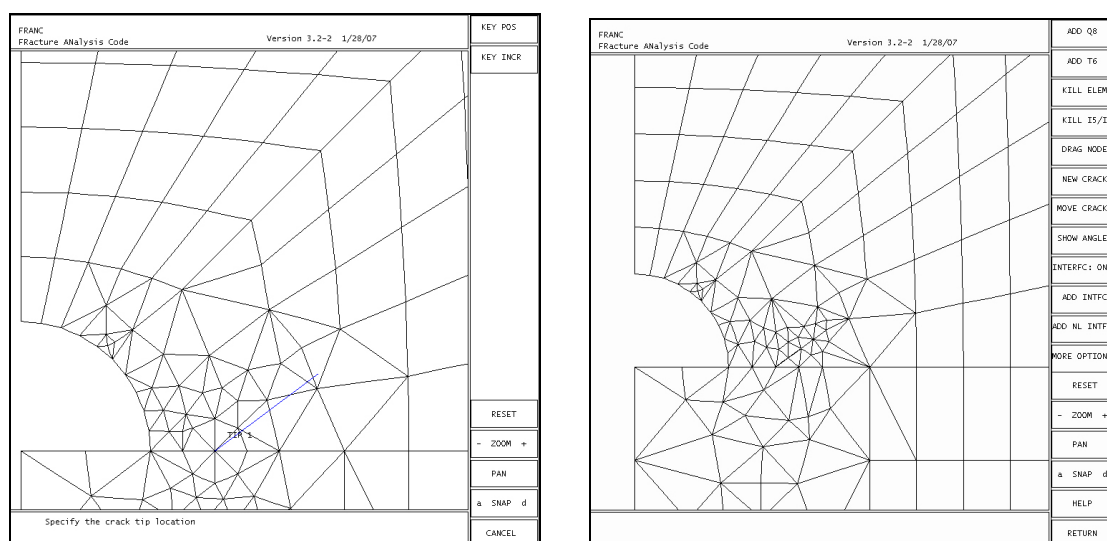

Fig. 6. (a) Propagation path at 2ⁿᵈ step   (b) Modified mesh with singular elements at crack tip
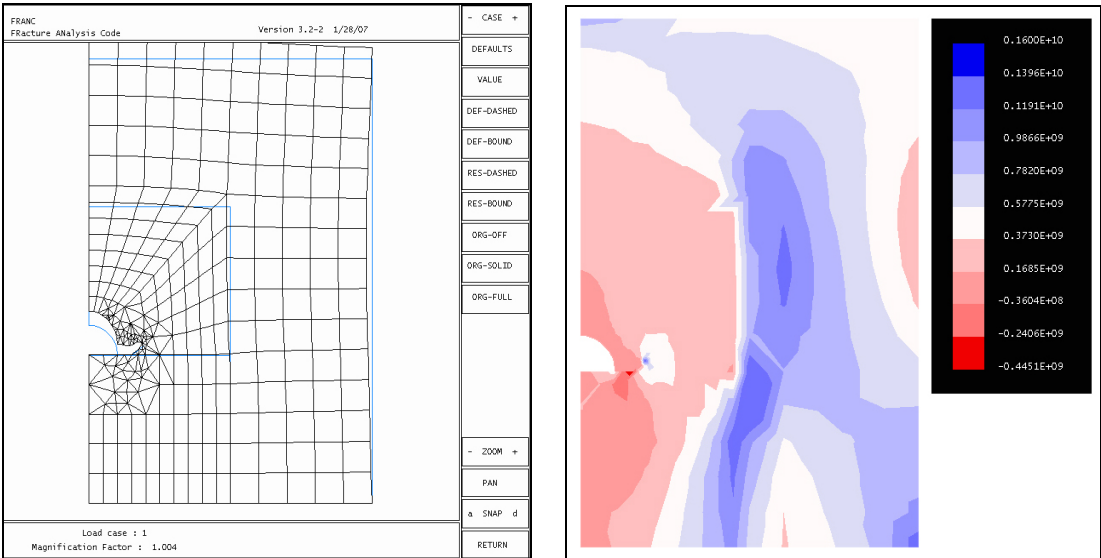
Fig. 7. (a) Deformed mesh at 2nd propagation step   (b) 1st principal stress at 2nd propagation step
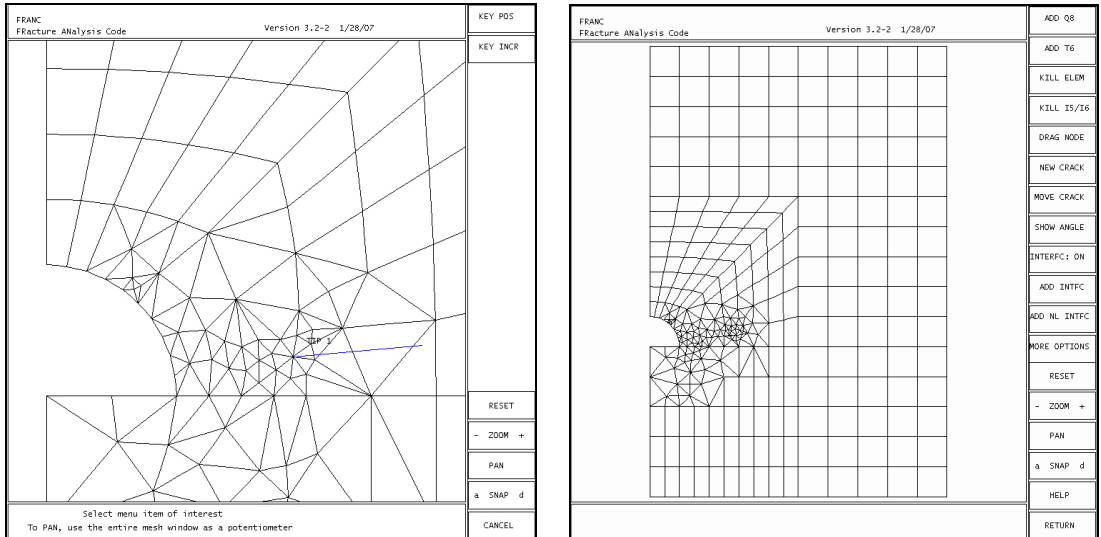
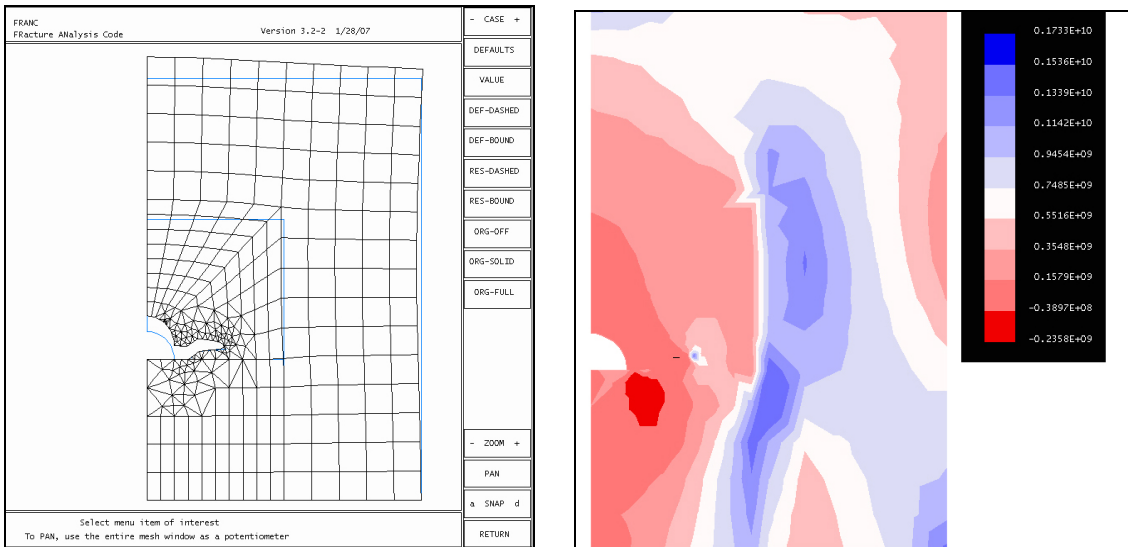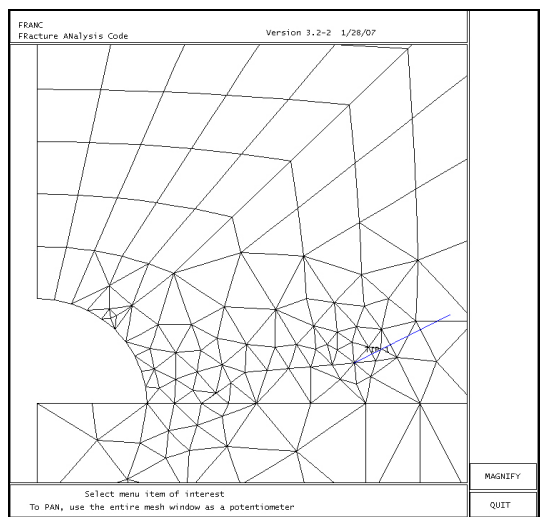**Fig. 8. (a) Propagation path at 3rd step   (b) Modified mesh with singular elements at crack tip**

Fig. 9. (a) Deformed mesh at 3rd propagation step   (b) 1st principal stress at 3rd propagation step
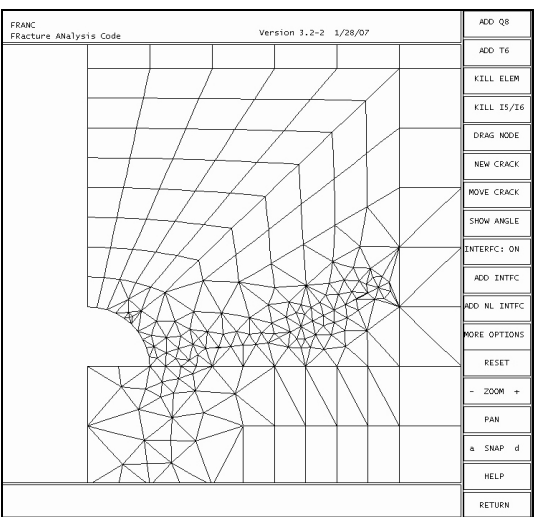
Fig. 10. (a) Propagation path at 4th step

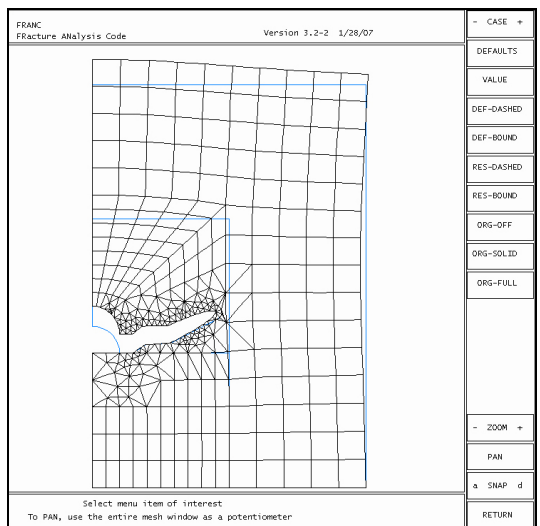
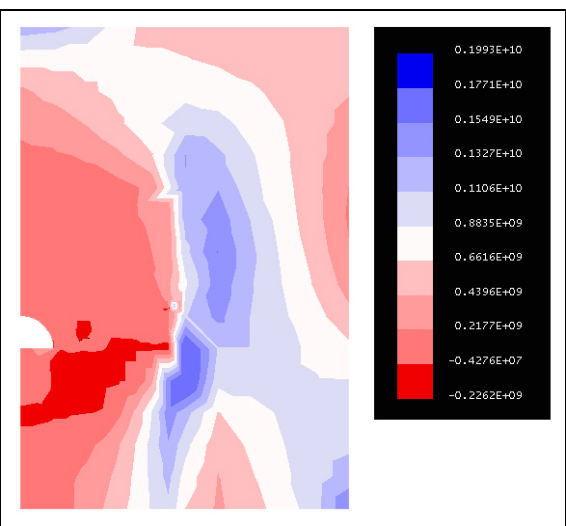**(b) Modified mesh with singular elements at crack tip**

Fig. 11. (a) Deformed mesh at 4th propagation step

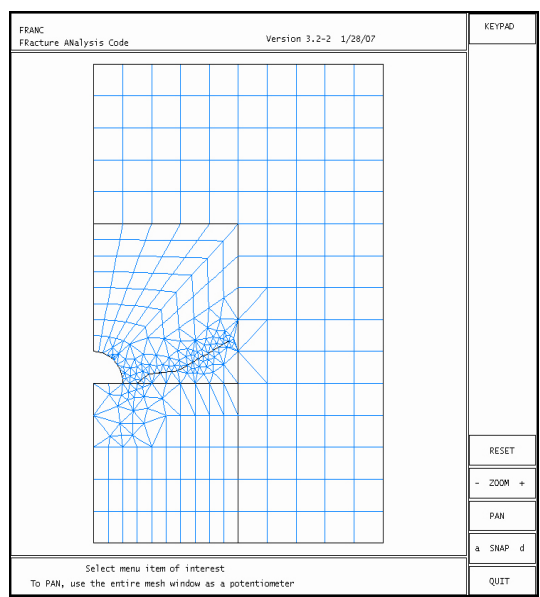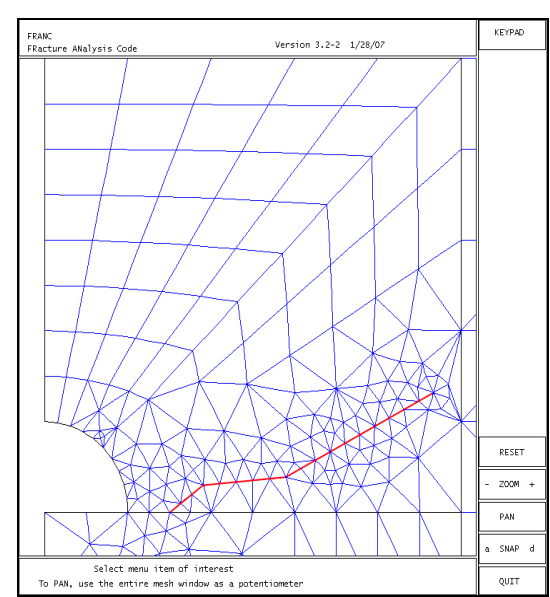**(b) 1st principal stress at 4th propagation step**

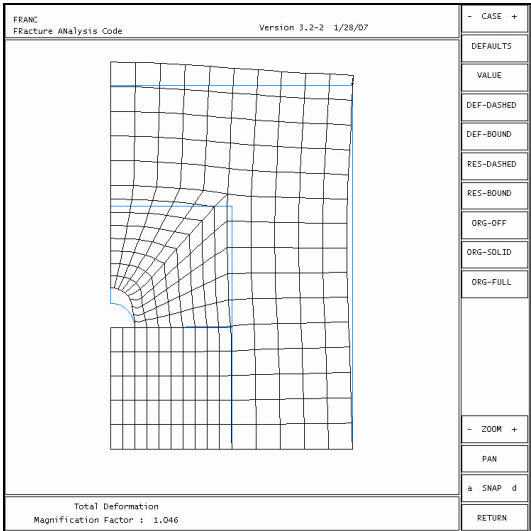**Fig. 12. Total crack propagation path**

Fig. 13. Deformed mesh with elastoplastic material behavior before crack formation

By considering elastoplastic material properties for acrylic cement and assuming the initial separation (first crack propagation path) at the cement-implant mating surface, the initial deformed shape, predicted propagation path, the first and last crack development steps and also the principal stresses contours are shown in Fig. 13 to Fig. 18.

5. Discussion

The rate of crack growth is usually separated into two categories.

One of those called stable crack growth is that propagates slowly with speed of e.g. 6.1 m/s (20 ft/s) and only propagate on application of an external load. The other category is fast growth with speed of e.g. 915m/s (3000 ft/s) and these cracks can proceed without external loading if there is sufficient internal elastic stressing (such as residual stresses from heat treating or crack propagation in a tensile sample after necking), this is referred as unstable crack growth [16]. In this study, stable crack growth was investigated because of assuming continuous application of external tensile load on surgical site during crack propagation.
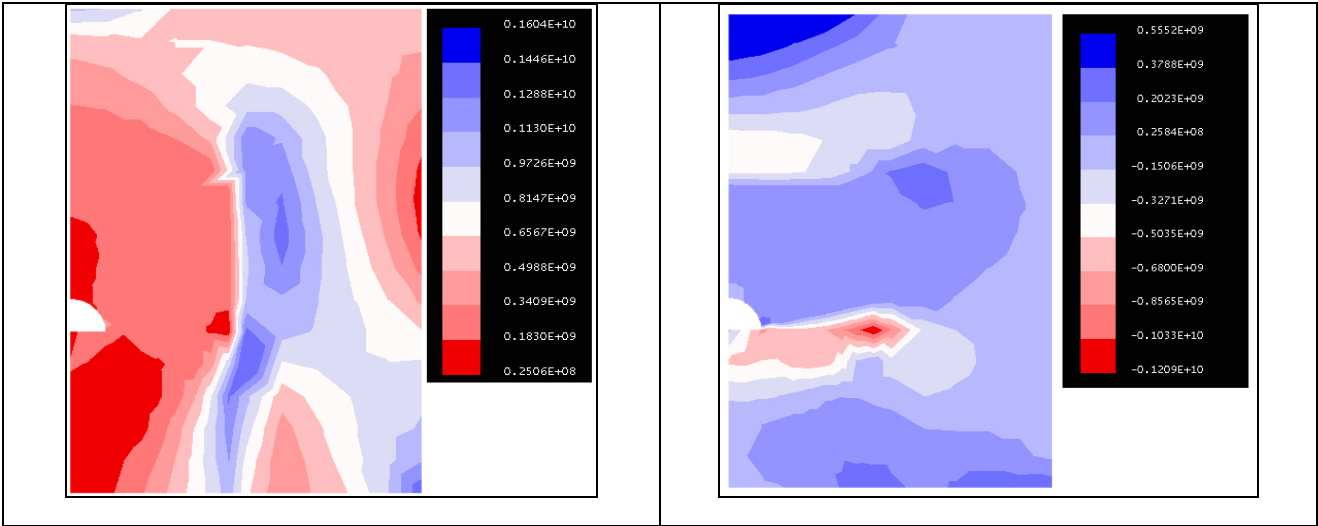

Fig. 14. (a) 1st principal stress at deformed state with elastoplastic material behavior before crack formation

(b) 2nd principal stress at deformed state with elastoplastic) material behavior before crack formation
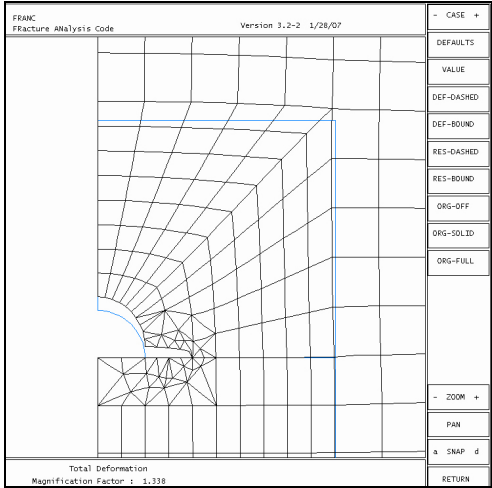

Fig. 15. Deformed mesh at 1st step of crack propagation with elastoplastic material behavior
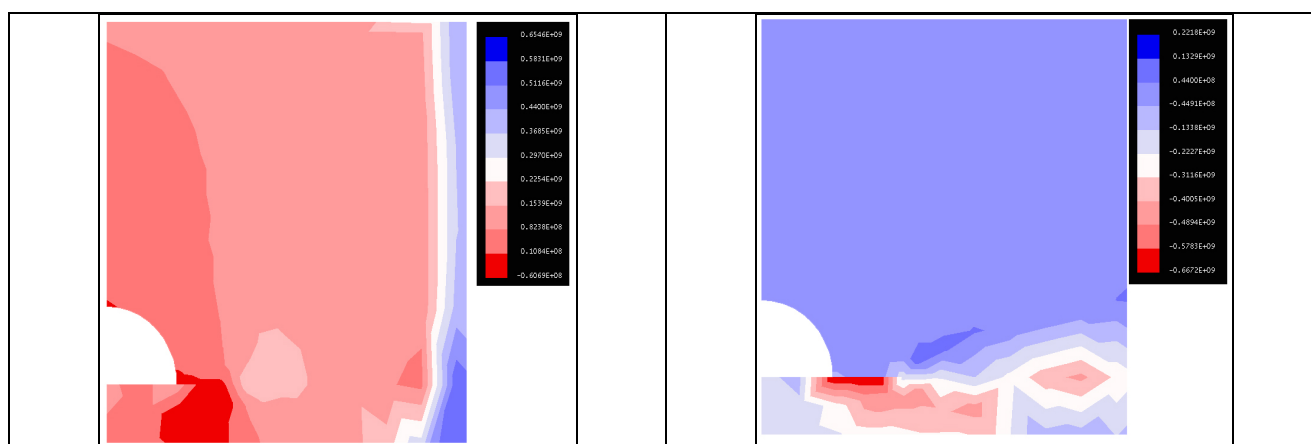
Fig. 16. (a) 1st principal stress at the 1st step of crack propagation with elastoplastic material behavior

(b) 2nd principal stress at the 1st step of crack propagation with elastoplastic material behavior

In first analysis when the bone cement is considered as purely elastic material, high stress levels can be seen at the crack tip in Fig. 5(b), Fig. 7(b), Fig. 9(b), and Fig.11(b).

The stresses acting at the crack tip locally exceed the strength of material if an elastoplastic material were used same as which was done at the second analysis and a plastic zone would be noticeable in the cement bulk as shown in Fig. 16 and Fig.18. However with an elastic material, in spite of that the initial separation path is considered at the cement-implant mating surface as shown in Fig. 4, but the crack propagation path was deviated from the interface and developed in to the cement structure that is shown in Fig.12. Secondly when an elastoplastic property is used for cement behavior, the initial separation path again considered along the interface as shown in Fig.15, but at the next steps the crack automatically developed along the interface and did not deviate much from it (Fig. 17).

Considering elastoplastic behavior for the cement structure better describes the cement-implant interface separation phenomenon due to presence of yielded elements around the crack tip in the cement structure and also low stress levels beneath the separation path in the implant, those are shown in Fig. 16 and Fig. 18 in 1st and 2nd principal stresses contours.

The results show that the crack can propagates either in the cement bulk or at the cement-implant interface depend on assumed material behavior and both of them could cause implant mechanical loosening. Both patterns have been seen frequently in clinical observations but the fracture pattern not only depends on the assumed material behavior but also depends on the amount of porosity of the material and cavities' volume fraction and moreover the interactions between the neighboring voids which may cause micro crack formation after transition of interface ligament necking between two neighboring voids under excessive external loading (see [7], [8], and [9]).
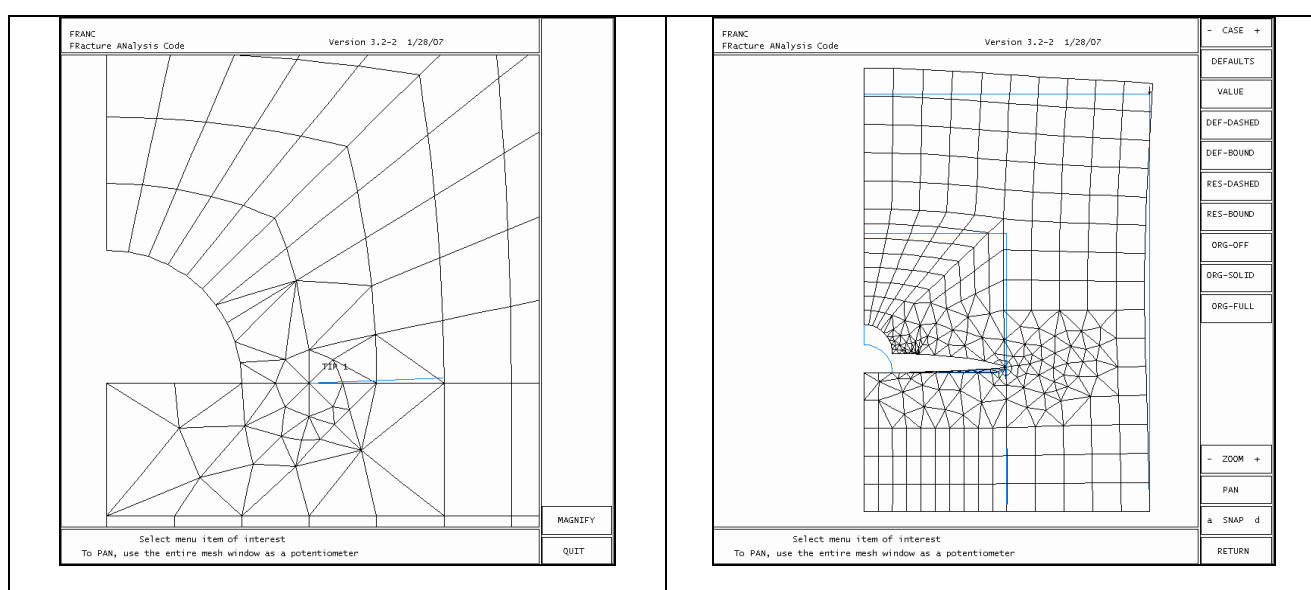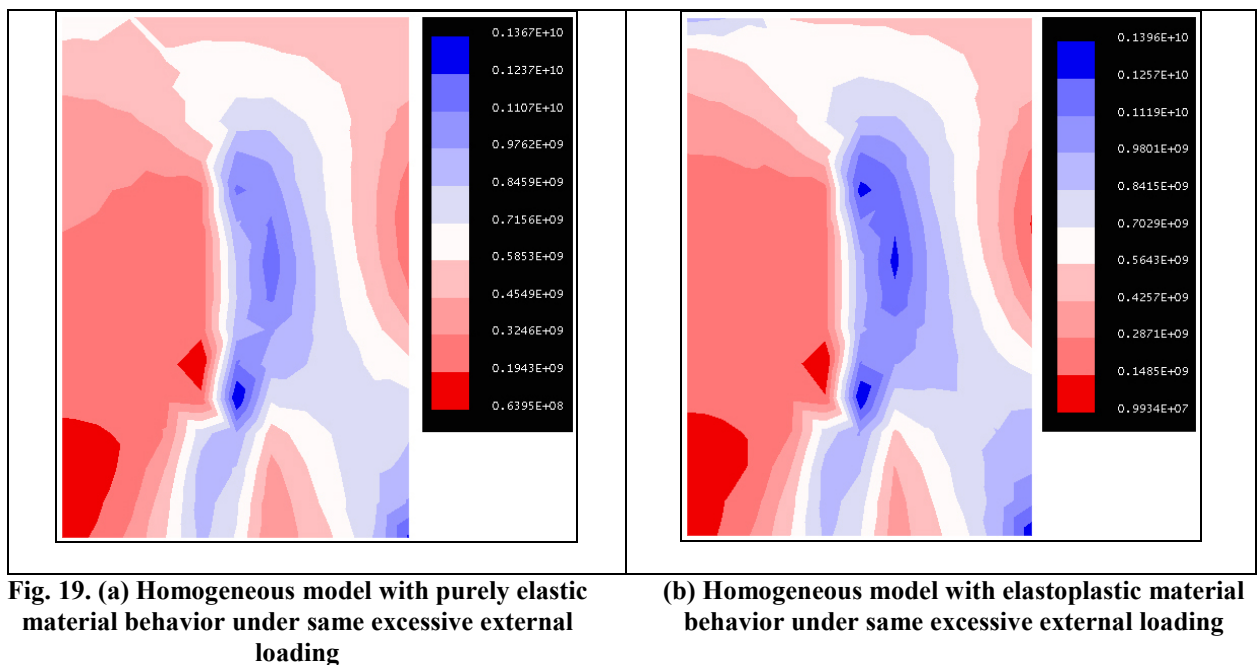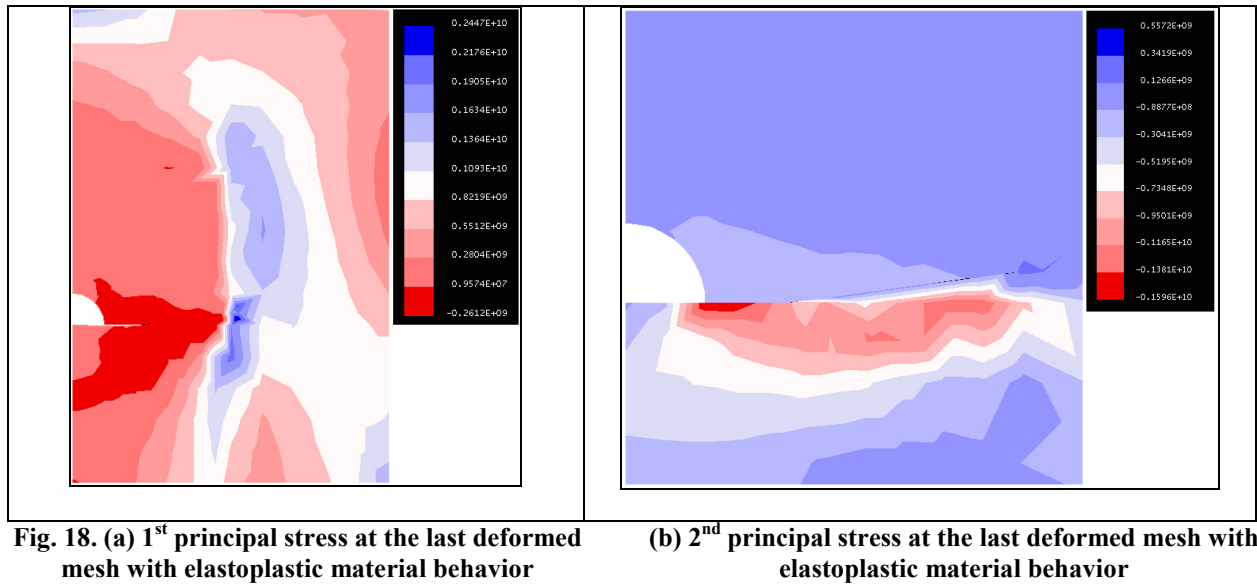

Fig. 17. (a) Software predicted propagation path

(b) Final deformed mesh

Fig. 18. (a) 1ˢᵗ principal stress at the last deformed mesh with elastoplastic material behavior

(b) 2ⁿᵈ principal stress at the last deformed mesh with elastoplastic material behavior

Fig. 19. (a) Homogeneous model with purely elastic material behavior under same excessive external loading

(b) Homogeneous model with elastoplastic material behavior under same excessive external loading

6. Conclusion

In the first part, the analytical investigation shows that there are no significant differences between homogeneous cement and inhomogeneous one when only a single spherical micro void with radius of 500μ exists in the cement bulk, but clinical and experimental observations and also fractography analyses show that the crack propagation and fracture occurred in cements which contain voids, pores and air bubbles. These outcomes (analytical solution and experimental observations) were not in accordance with each other. So, to solve this paradox in low porosity materials, in which changes between homogeneous and inhomogeneous material properties are small enough, a numerical simulation is performed to evaluate stress concentration effect due to presence of a single void or dilutely dispersed voids.

As shown in numerical analysis, the stress concentrations due to presence of inhomogeneities including voids and cavities form an appropriate site for crack nucleation and stable crack growth under applied external loading that leads to cement fracture, but as studied in analytical solution, with current void size and its volume fraction there are no significant changes in material elasticity & yield stress and the differences between homogenous orthopedic cement and inhomogeneous one in both properties are less than one percent. So, it is concluded that the stress concentration due to irregular discontinuity in the material structure is more effective than its resultant strength reduction. E.g. the results from a homogeneous model (Fig. 19) show a uniform stress distribution in the cement structure with the range of $0.1485E9 \sim 0.2871E9$ N/m² for 1ˢᵗ principal stresses of

elastoplastic material behavior, but when an inhomogeneity like a semi spherical macro void with radius of 500μ is considered at the interface, as modeled in this study, with same elastoplastic material behavior, the stresses in the cement structure rise up to $0.1830E9 \sim 0.3409E9$ N/m^2 , and also a stress concentration zone forms in which the stresses are in the range of $0.3409E9 \sim 0.4988E9$ N/m^2 , which approximately are 2 times more than those in homogenous material.

So it is concluded that not only the inhomogeneities (i.e. voids and cavities) in the cement structure affect the material strength, but also they form stress concentration zones in the material structure. Even if the void's volume fraction is small enough, as in this analysis, that does not affect much the material strength, but because of stress concentration and high local stress levels, a proper site for crack nucleation will be formed. High Vacuum Mixing helps to reduce the cement porosity and increases the strength of orthopedic cement and long term stability of cemented implants. It should be noted that, the fracture pattern in the cement structure not only determined by cement material properties but also depends on the amount of porosity of the material and interaction between the voids and also the size of the neighboring voids.

References

[1] Walencamp, G., Murray, D., *"Bone Cements and Cementing Technique"*, Springer Verlag, 2001

[2] Lidgren, L., Drar, H., Möller, J., *"Strength of Polymethylmethacrylate Increased By Vacuum Mixing"*, Acta Orthop. Scand., Vol. 55, 1984, pp 536 541.

[3] Alkire, M.J., Dabezies, E.J., Hastings, P.R., *"High Vacuum As a Method of Reducing Porosity of Polymethylmethacrylate"*, J. Orthopedics, Vol.10, 1987, pp.1533 1539

[4] Bishop, N., Fergusen, S., Tepic, S., *"Porosity Reduction in Bone Cement at Cement-Stem Interface"*, JBJS, Vol. 78, 1996, pp 349 356, JBJS.

[5] Harrigan, T.P., Harris, W.H., *"A Three Dimensional Nonlinear Finite Element Study of the Effect of Cement-Prosthesis Debonding in Cemented Total Hip Component,"* Journal of Biomechanics, Vol.24, 1991, pp. 1047 1058.

[6] Jasty, M., Maloney, W.J., Bragdon, C.R., O'Connor, D., Haire, T., Harris, W.H.,"*The Initiation of Failure in Cemented Femoral Components of Hip Arthroplasties,*" Journal of Bone and Joint Surgery, Vol.73B, 1991, pp. 551 558.

[7] Tvergaard, V., *"Interface Failure By Cavity Growth to Coalescence"*, Int. J. Mechanical Sciences, Vol. 42, 2000, pp. 381 395.

[8] Tvergaard, V., *"Studies of Void Growth in a Thin Ductile Layer between Ceramics"*, J. Computational Mechanics, Vol. 20, 1997, pp 186 191.

[9] Tvergaard, V., *"Interaction of Very Small Voids with Larger Voids"*, Int. J. Solid Structures, Vol. 35, 1998, pp. 3989 4000

[10] Mura, T., *"Micromechanics of Defects in Solids,"* Martinus Nijhoff, Netherlands, 1982.

[11] Bohm, H. J., *"A Short Introduction to Basic Aspects of Continuum Micromechanics,"* CDL-FMD-Report, hjb/ILSB 060521, ILSB Vienna University of Technology, 2006.

[12] Huiskes, R., *"Some Fundamental Aspects of Human Joint Replacement"*, Acta Orthopedica Scandinaviea Supplement, 1980, pp 185 208.

[13] Nuno, N., Avanzolini, G., *"Residual Stresses at Stem-Cement Interface of an Idealized Cement Hip Stem"*, J. of Biomechanics, Vol. 35, 2002, pp. 849 852.

[14] Panjabi, M., White, A., *"Biomechanics in the Musculoskeletal System"*, Churchill Livingstone Pub. 2004.

[15] Katoozian, H., Davy, D. T., Arshi, A., Saadati, Y., *"Material Optimization of Femoral Component of Total Hip Prosthesis Using Fiber Reinforced Polymeric Composites"*, J. Medical Engineering & Physics, Vol. 23, 2001, pp. 503 509.

[16] Brooks, C., Choudhury, A., "Failure Analysis of Engineering Materials", Mc Graw-Hill Pub., 2002.

Nomenclature

C_{ijkl}	Elastic modulus of infinitely extended material
C_{ijkl}^*	Elastic modulus of inhomogeneity
$D(\underline{n})$	Determinant of stiffness matrix
$\mathbf{E}_M^*$	Effective elasticity tensor by Mori-Tanaka estimation theorem
$\mathbf{E}^{(m)}$	Matrix elasticity tensor
$\mathbf{E}^{(i)}$	Inclusion elasticity tensor
$\mathbf{I}$	Identity matrix
k	Bulk modulus
n	Outward normal
$N_{kp}(\underline{n})$	Cofactor of stiffness matrix
S_{ijkl}	Eshelby tensor
u_i	Displacement disturbance
$u_{i,j}^0$	Displacement gradient
δ_{ij}	Kronecker δ
ε_{ij}^0	Strain due to applied stress at infinity
ε_{ij}^*	Eigen strain
λ	Lame constant
μ	Lame constant
σ_{ij}	Stress disturbance
σ_{ij}^0	Applied stress at infinity

ν Poisson's ratio

Ω^{i} Volume of inclusion

Ω^{m} Volume of matrix

ξ Void (inhomogeneity) volume fraction

Expressions for Eshelby tensor of ellipsoidal inclusions in an isotropic matrix are given here.

Appendix A

$$S_{1111} = S_{2222} = S_{3333} = \frac{7 - 5\nu}{15(1 - \nu)}$$

$$S_{1122} = S_{2233} = S_{3311} = S_{1133} = S_{2211} = S_{3322} = \frac{5\nu - 1}{15(1 - \nu)}$$

$$S_{1212} = S_{2323} = S_{3131} = \frac{4 - 5\nu}{15(1 - \nu)}$$